Imaging of C-X-C motif chemokine receptor 4 expression in 690 patients with solid or hematologic neoplasms using 68Ga-Pentixafor PET

Andreas K. Buck, Alexander Haug, Niklas Dreher, Alessandro Lambertini, Takahiro Higuchi, Constantin Lapa, Alexander Weich, Martin G. Pomper, Hans-Jürgen Wester, Anja Zehnder, Andreas Schirbel, Samuel Samnick, Marcus Hacker, Verena Pichler, Stefanie Hahner, Martin Fassnacht, Hermann Einsele, Sebastian Serfling, Rudolf A. Werner

Angaben zur Veröffentlichung / Publication details:

Buck, Andreas K., Alexander Haug, Niklas Dreher, Alessandro Lambertini, Takahiro Higuchi, Constantin Lapa, Alexander Weich, et al. 2022. "Imaging of C-X-C motif chemokine receptor 4 expression in 690 patients with solid or hematologic neoplasms using 68Ga-Pentixafor PET." *Journal of Nuclear Medicine* 63 (11): 1687–92. https://doi.org/10.2967/jnumed.121.263693.

Imaging of C-X-C Motif Chemokine Receptor 4 Expression in 690 Patients with Solid or Hematologic Neoplasms Using ^{68}Ga-Pentixafor PET

Andreas K. Buck*[1], Alexander Haug*[2], Niklas Dreher[1], Alessandro Lambertini[1], Takahiro Higuchi[1,3], Constantin Lapa[4], Alexander Weich[5], Martin G. Pomper[6], Hans-Jürgen Wester[7], Anja Zehndner[1,8], Andreas Schirbel[1], Samuel Samnick[1], Marcus Hacker[2], Verena Pichler[9], Stefanie Hahner[10], Martin Fassnacht[10], Hermann Einsele[11], Sebastian E. Serfling†[1], and Rudolf A. Werner†[1,6]

[1]Department of Nuclear Medicine, University Hospital Würzburg, Würzburg, Germany; [2]Division of Nuclear Medicine, Medical University of Vienna, Vienna, Austria; [3]Okayama University Graduate School of Medicine, Dentistry and Pharmaceutical Sciences, Okayama, Japan; [4]Nuclear Medicine, Medical Faculty, University of Augsburg, Augsburg, Germany; [5]Department of Internal Medicine II, Gastroenterology and ENETS Center of Excellence, University Hospital Würzburg, Würzburg, Germany; [6]The Russell H Morgan Department of Radiology and Radiological Sciences, Johns Hopkins School of Medicine, Baltimore, Maryland; [7]Pharmaceutical Radiochemistry, Technische Universität München, München, Germany; [8]Pentixapharm Würzburg, Würzburg, Germany; [9]Division for Pharmaceutical Chemistry, Medical University of Vienna, Vienna, Austria; [10]Division of Endocrinology and Diabetes, Department of Medicine I, University Hospital, University of Würzburg, Würzburg, Germany; and [11]Department of Internal Medicine II, Hematology and Oncology, University Hospital Würzburg, Würzburg, Germany

For correspondence or reprints, contact Andreas K. Buck (buck_a@ukw.de).
*Contributed equally to this work.
†Contributed equally to this work.

Because of its pivotal role in cancer progression, the C-X-C motif chemokine receptor 4 (CXCR4) orchestrates organ-specific tumor spread through several mechanisms. These include promotion of angiogenesis, growth of malignant cells, or inhibition of antitumor immune response (*1*). Numerous CXCR4-directed molecular imaging agents have been developed recently to define precisely the utility of CXCR4 as an anticancer target (*2–5*). Among them, the ^{68}Ga-labeled radiotracer Pentixafor (cyclo(D-Tyr^1-D-[NMe]Orn^2(AMBS-^{68}Ga-DOTA)-Arg^3-Nal^4-Gly^5) demonstrated high selectivity for CXCR4 along with rapid renal excretion (*6,7*). Accordingly, ^{68}Ga-Pentixafor has been used in a wide variety of clinical scenarios in oncology. These include in patients with multiple myeloma (MM), marginal zone lymphoma or solid tumor entities, such as small-cell lung cancer (SCLC) and non–small cell lung cancer, neuroendocrine neoplasms, and adrenocortical carcinoma (*8–13*). Of note, head-to-head comparison with established imaging modalities or other reference radiotracers revealed improved lesion detection rates by ^{68}Ga-Pentixafor PET (*8,14,15*). This may promote wider adoption of this imaging agent in patients for whom existing modalities are lacking. Furthermore, ^{177}Lu/^{90}Y-Pentixather, a therapeutic counterpart to target CXCR4, has been applied for targeted radionuclide therapies in hematologic malignancies, such as MM or diffuse large B cell lymphoma (*16,17*). Such theranostic approaches have demonstrated not only a favorable outcome (*16,17*), but also tolerable adverse effects, although stem cell support is mandatory (*18*).

The beneficial use of ^{68}Ga-Pentixafor PET/CT, along with its potential to identify patients eligible for treatment with β-particle emitters, favors wider clinical use. However, before widespread adoption or clinical development programs leading to market authorization, comprehensive characterization of its performance should be undertaken,

including assessment of radiopharmaceutical uptake and image contrast among a broad spectrum of neoplasms. In our bicentric study, which, to our knowledge, enrolled the largest cohort of patients imaged with ^{68}Ga-Pentixafor PET/CT or PET/MR to date, we aimed to assess radiopharmaceutical accumulation and image contrast in several cancers to determine the most relevant clinical applications. In addition, lower specific activity characterized by higher amounts of cold mass could hamper image interpretation (*19*), for example, by an increasing occupation of the (sub)cellular target by nonradiolabeled components. Thus, we also investigated the impact of specific activity on quantification.

MATERIALS AND METHODS

Patient Population

Patients from 2 study sites were included (University of Würzburg and Medical University of Vienna). Parts of this cohort have been described before to determine the diagnostic usefulness of ^{68}Ga-Pentixafor PET/CT (*7–9,11–14,20–26*), without evaluation of image contrast (including impact of specific activity) or comparing uptake among all included diagnoses. Patients signed written informed consent forms before the examination. Given the retrospective character of this study, the local ethics committee waived the need for further approval (no. 20210726 02).

Radiotracer Synthesis

Following good manufacturing practice, ^{68}Ga-Pentixafor was provided using a synthesis module (Scintomics) and disposable single-use cassette kits (ABX, Radeberg, Germany), as described previously (*27*). Peptide mass (in μg), activity (in MBq), and specific activity (in MBq/μg) of injected ^{68}Ga-Pentixafor were recorded for each patient.

Imaging

^{68}Ga-Pentixafor PET was performed either on a Siemens Biograph mCT (64 and 128, Siemens Medical Solutions) or on a Siemens Biograph mMR (Siemens Healthcare GmbH). Whole-body scans (covering the vertex of the skull to the proximal thighs) were conducted 60 min after injection of ^{68}Ga-Pentixafor. We also performed low-dose CT scanning for attenuation correction and anatomic coregistration (120 keV, 512 × 512 matrix, 5-mm slices, increment: 30 mm/s, pitch index: 0.8, and rotation time: 0.5 s). PET images were reconstructed including corrections for CT-based attenuation, random events, and scatter. For MRI, we applied an integrated radiofrequency coil including a multistation protocol (slice thickness, 2 mm), as previously described (*12,28*).

Image Interpretation

All scans were obtained for clinical or research purposes. As part of this study, all images were reanalyzed by readers who were masked to respective clinical information. At Würzburg, image interpretation was performed as a single-reader analysis, verified by an expert reader. At Vienna, an expert reader performed the assessment.

Semiquantitative Assessment. A target lesion (TL) assessment was performed by investigating the visually most intense TL on PET. Three-dimensional volumes of interest applying an isocontour threshold of 40% were placed on the TL, providing SUV_{max}, SUV_{mean}, and SUV_{peak}. A target–to–blood-pool ratio (TBR) was derived by placing a volume of interest over the aortic arch. TBR was then provided by dividing SUV_{max} (of the TL) by SUV_{mean} (of the blood pool) (*12*).

Statistical Analysis

Statistical analysis was performed using GraphPad Prism (version 9.2.0, GraphPad Prism Software). Descriptive results are displayed as mean ± SD. Nonparametric Spearman correlation coefficients were calculated to investigate associations between semiquantitative parameters with specific activity (including an outlier correction using the ROUT-Method). A P value of less than 0.05 was considered statistically significant.

RESULTS

Highest Uptake in Hematologic Malignancies, SCLC, and Adrenocortical Neoplasms

No adverse events were recorded after injection of ^{68}Ga-Pentixafor. Two hundred forty-two of 777 (31.1%) of the scans did not show discernible uptake, leaving 535 of 777 (68.9%) cases for further analysis (Table 1). As such, an overall number of 535 TLs were investigated. Among all TLs, SUV_{max} was 13.01 ± 10.01 and the corresponding TBR was 8.59 ± 15.98. The highest average SUV_{max} (>12) was found in MM (n = 113), followed by adrenocortical carcinoma (n = 30), mantle cell lymphoma (MCL; n = 20), adrenocortical adenoma (n = 6), and SCLC (n = 12; Figs. 1 and 2). The lowest average SUV_{max} (<6) was recorded in osteosarcoma (n = 1), followed by bladder cancer (n = 1),

TABLE 1
Overview of Positive ^{68}Ga-Pentixafor PET Scans and Individual Diagnoses of Patients Included

Diagnosis	No. of scans
Marginal zone lymphoma	187 (35)
Multiple myeloma	113 (21.1)
Chronic lymphocytic leukemia	50 (9.3)
Adrenocortical carcinoma	30 (5.6)
Neuroendocrine neoplasm	30 (5.6)
Mantle cell lymphoma	20 (3.7)
Desmoplastic small round cell tumor	14 (2.6)
Myeloid disorders	13 (2.4)
Small cell lung carcinoma	12 (2.2)
B-cell lymphoma	10 (1.9)
Acute myeloid leukemia	9 (1.7)
Pancreas carcinoma	8 (1.5)
Non–small cell lung carcinoma	7 (1.3)
Adrenocortical adenoma	6 (1.1)
Acute lymphoblastoid leukemia	6 (1.1)
Liver carcinoma	4 (0.7)
T-cell lymphoma	3 (0.6)
Cholangiocarcinoma	3 (0.6)
Head and neck cancer	2 (0.4)
Colorectal cancer	1 (0.2)
Pleural mesothelioma	1 (0.2)
Renal cell carcinoma	1 (0.2)
Ovarian cancer	1 (0.2)
Ewing sarcoma	1 (0.2)
Osteosarcoma	1 (0.2)
Mediastinal tumor*	1 (0.2)
Bladder cancer	1 (0.2)

*Not otherwise specified.
Data in parentheses are percentages.

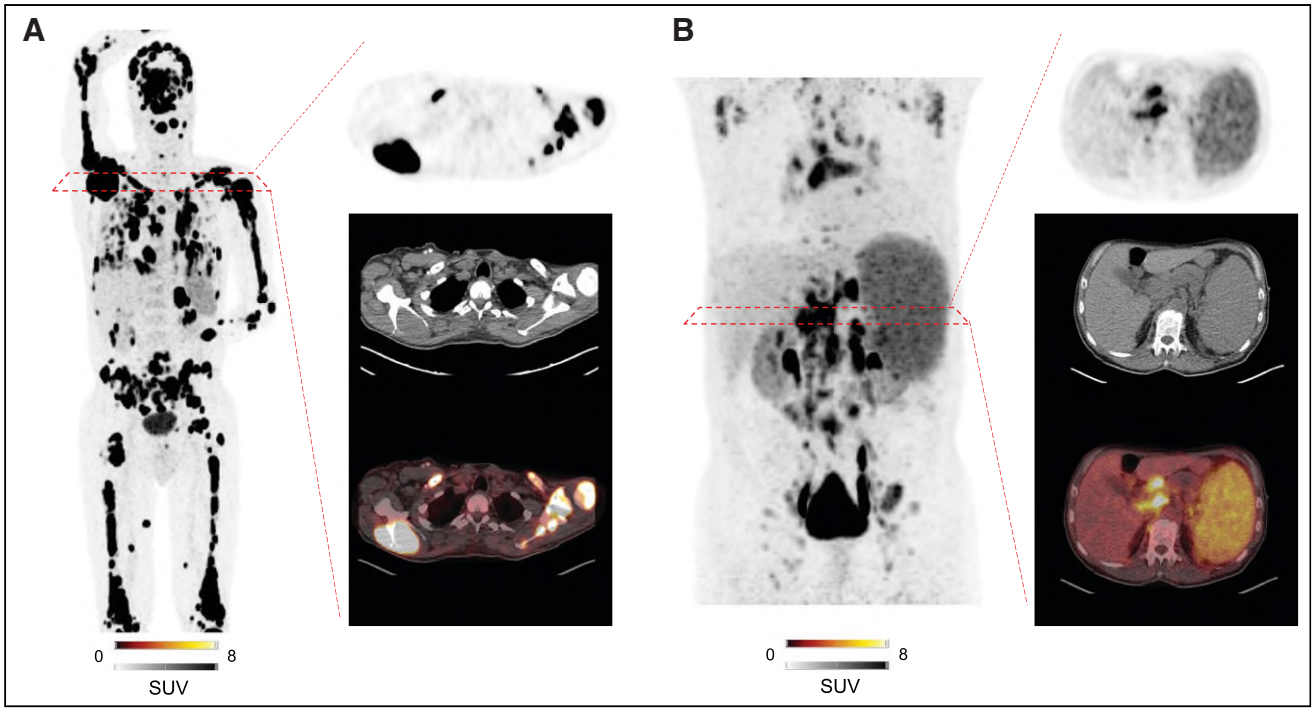

FIGURE 1. Maximum-intensity projections of patients with hematologic malignancies imaged with CXCR4-directed ^{68}Ga-Pentixafor. Target lesion is also displayed on transaxial PET, CT, and PET/CT. Patient diagnosed with MM (A; SUV_{max} in target lesion, 74.3) and MCL (B; SUV_{max} in target lesion, 17.2). Substantially low background activity allowed for precise determination of disease sites.

mediastinal tumor (not otherwise specified, $n = 1$), head and neck cancer ($n = 2$), and Ewing sarcoma ($n = 1$; Fig. 3). For SUV_{peak}, comparable results were achieved (Supplemental Fig. 1). Moreover, high average TBR (>8) was recorded in MM, MCL, and acute lymphoblastoid leukemia ($n = 6$). Low average TBR (<4) was observed in head and neck cancer, colorectal cancer ($n = 1$), osteosarcoma, Ewing sarcoma, bladder cancer, renal cell carcinoma ($n = 1$), and mediastinal tumor (Fig. 4).

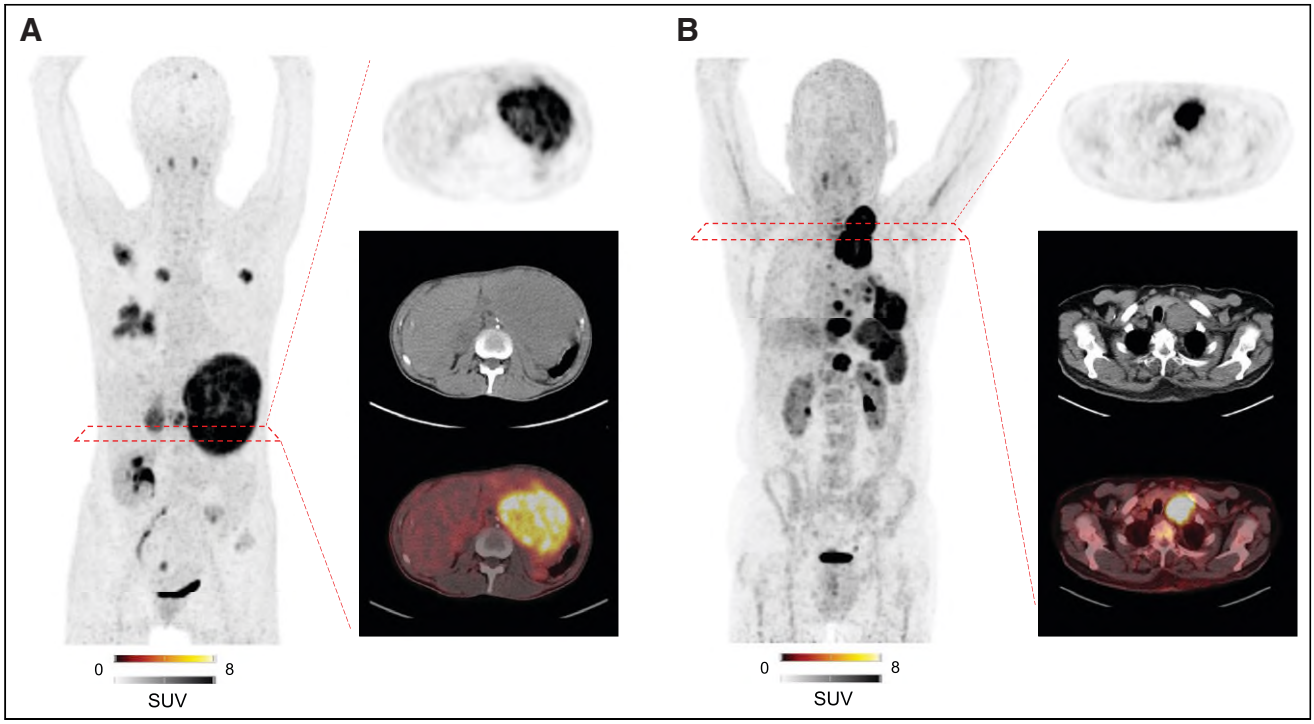

FIGURE 2. Maximum-intensity projections of patients with solid tumor entities imaged with CXCR4-directed ^{68}Ga-Pentixafor. Target lesion is also displayed on transaxial PET, CT, and PET/CT. Patient diagnosed with adrenocortical carcinoma (A; SUV_{max} in target lesion, 13.2) and small cell lung carcinoma (B; SUV_{max} in target lesion, 19.4). Background activity was substantially low, providing a precise read-out of disease sites.

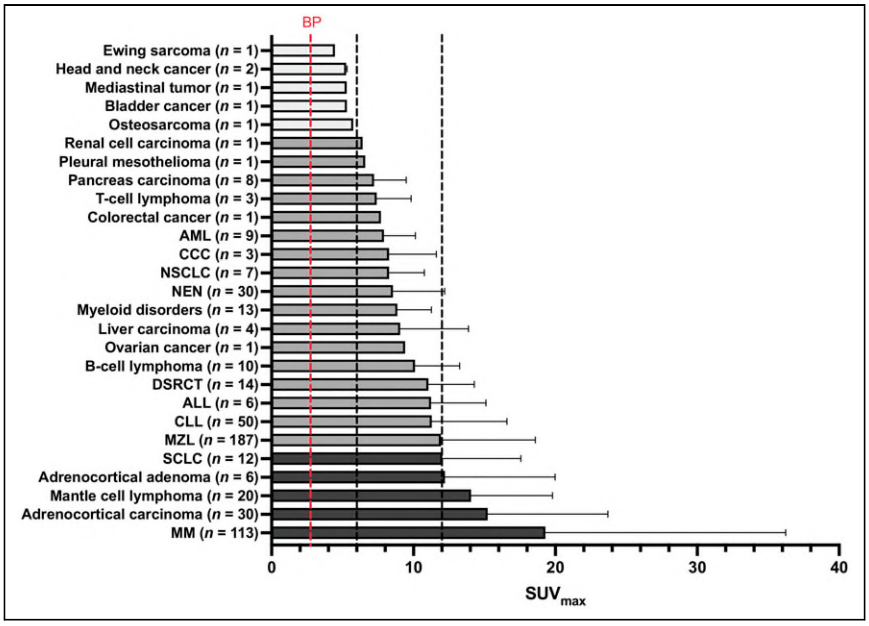

FIGURE 3. Bar chart displaying average SUV_{max}. Mean ± SD is indicated. Black dotted lines show SUV_{max} cutoffs of 6 and 12, respectively. BP = blood pool (red dotted line); AML = acute myeloid leukemia; CCC = cholangiocarcinoma; NSCLC = non–small cell lung carcinoma; NEN = neuroendocrine neoplasm; DSRCT = desmoplastic small round cell tumor; ALL = acute lymphoblastoid leukemia; CLL = chronic lymphocytic leukemia; MZL = marginal zone lymphoma; SCLC = small cell lung carcinoma; MM = multiple myeloma. In individual lesions, a markedly increased SUV_{max} of up to 85.8 was observed. Number of investigated patients (*n*) per diagnosis group is given in parentheses.

No Relevant Impact of Specific Activity on Visual or Semiquantitative Assessment

Median injected peptide mass was 8.5 μg (range, 2.56–35.61 μg), injected activity was 143 MBq (range, 38–239 MBq), and specific activity was 15.39 MBq/μg (range, 2.19–43.70 MBq/μg). Comparing specific activity with semiquantitative parameters, only SUV_{mean} ($\rho = -0.138$, $P = 0.002$), but none of the other correlative indices, reached significance (SUV_{max}: $\rho = 0.01$, $P = 0.832$; TBR: $\rho = 0.023$, $P = 0.612$; SUV_{peak}: $\rho = -0.087$, $P = 0.053$; Fig. 5).

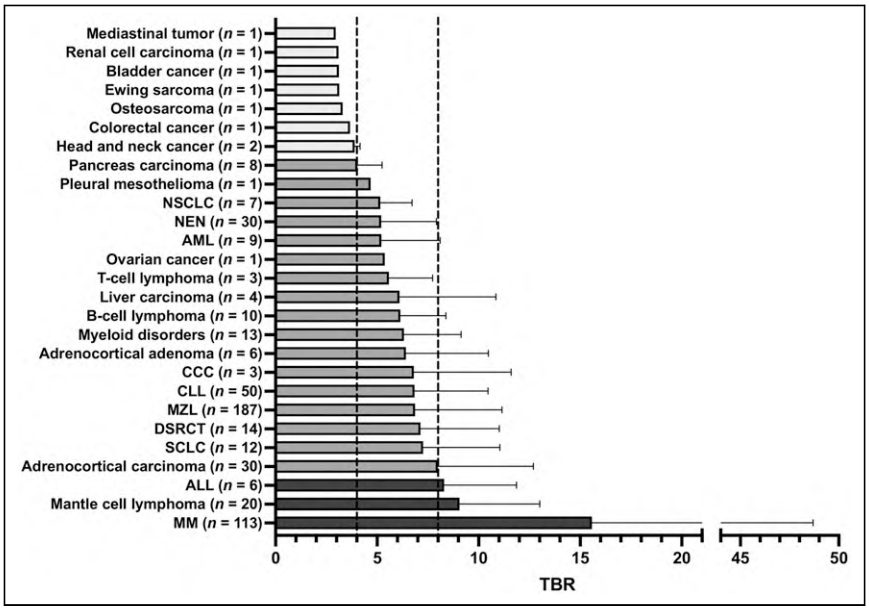

FIGURE 4. Bar chart displaying average TBR. Mean ± SD is indicated. Black dotted lines show TBR cutoffs of 4 and 8, respectively. NSCLC = non–small cell lung carcinoma; NEN = neuroendocrine neoplasm; AML = acute myeloid leukemia; CCC = cholangiocarcinoma; CLL = chronic lymphocytic leukemia; MZL = marginal zone lymphoma; DSRCT = desmoplastic small round cell tumor; SCLC = small cell lung carcinoma; ALL = acute lymphoblastoid leukemia; MM = multiple myeloma. Number of investigated patients (*n*) per diagnosis group is given in parentheses.

DISCUSSION

In the present bicentric study investigating a large cohort imaged with ^{68}Ga-Pentixafor, discernible uptake in putative sites of disease was noted in more than 68% of the scans. Among neoplasms studied, we determined MM had the highest uptake (SUV), with adrenocortical carcinoma and MCL closely after. Comparable results were recorded for image contrast (TBR). Specific activity had no impact on a semiquantitative level, supporting the notion that an excellent read-out can be achieved, even after administration at low specific activities.

A growing body of evidence supports the clinical utility of CXCR4-targeted ^{68}Ga-Pentixafor PET/CT in a variety of disease entities, including hematologic malignancies (*7,22*) and solid tumors (*29*). Some of these studies also revealed that ^{68}Ga-Pentixafor provided an increased detection rate at sites of disease when compared with conventional imaging or other PET agents such as ^{18}F-FDG or somatostatin receptor–directed radiopharmaceuticals, thereby indicating that this agent can image malignancies that lack a more suitable modality (*15,23,26*). Here we aimed to provide a precise cohort of neoplasms that exhibit high tracer avidity and excellent TBR. By investigating 690 patients with 35 different types of cancer, we demonstrated that ^{68}Ga-Pentixafor PET exhibits the most intense uptake in hematologic malignancies, such as MM, MCL, or acute lymphoblastoid leukemia. ^{68}Ga-Pentixafor PET did not perform as well in solid tumors. Nevertheless, a TBR of more than 4 was still achieved in certain cases, for example, adrenal, SCLC, liver, ovarian, neuroendocrine neoplasms, or pancreatic cancer (Fig. 4). We also checked whether low specific activity may have hampered image contrast (*19*), for example, by an increasing occupancy of the target by carrier. However, we ruled out a relevant impact on a semiquantitative level (Fig. 5). This is also in line with previous affinity studies, demonstrating that ^{68}Ga-Pentixafor completely interacts with the binding pocket of CXCR4 (*30*). Nonetheless, novel second-generation radiotracers based on *iodo*CPCR4 analogs with altered linker structure may further increase tumor retention (*31*).

Increased CXCR4 expression on the tumor cells has been tightly linked to poor outcome in hematologic malignancies and

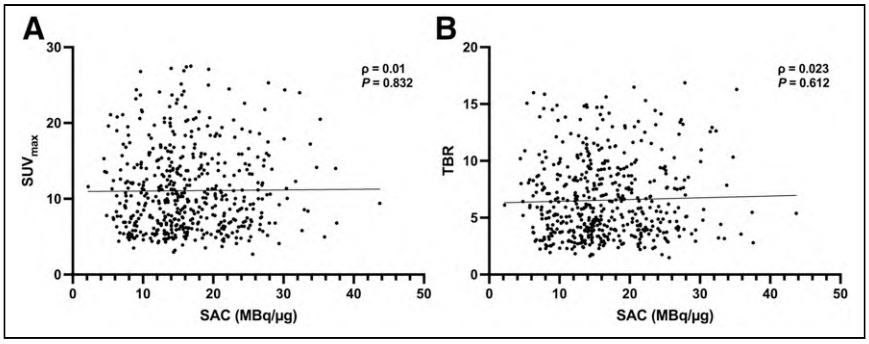

FIGURE 5. Correlation plots between specific activity in MBq/μg and SUV_{max} (A) and TBR (B). Significant Spearman ρ and *P* are displayed. No significance was reached.

solid tumors (*32,33*), suggesting it as a viable therapeutic target. For example, the stromal cell–derived factor 1 neutralizing agent Olaptesed pegol (NOX-A12) or the CXCR4 antagonist Plerixafor have each been used in patients with refractory MM. In clinical phase I/II studies, such drugs achieved an overall response rate in almost half of the patients (Plerixafor) or partial response in 68% (NOX-A12) (*34,35*). Theranostic approaches based on ^{68}Ga-Pentixafor scan results have also been conducted using the therapeutic analogs ^{177}Lu/^{90}Y-Pentixather (*16,18*). Although there is no study reporting an association between PET-based SUV_{max} and absorbed doses in lesions on CXCR4-directed imaging and radionuclide therapies to date, the markedly increased SUV_{max} observed in certain cases suggests that a substantial fraction of patients may also be eligible for CXCR4-directed radioligand therapies. However, CXCR4-targeted endoradiotherapy causes bone marrow ablation and, thus, subsequent stem cell support is needed (*18*), further emphasizing the importance of well-established algorithms for adequate patient selection.

Future studies should also evaluate the ability of CXCR4-directed molecular imaging to assess the retention capacities of nonradiolabeled CXCR4 neutralizing agents in vivo, preferably before treatment onset. For instance, a phase I study evaluating the CXCR4 inhibitor LY2510924 in patients with advanced solid cancers revealed favorable antitumor activity (*36*). Of note, a substantial patient fraction treated with this "cold" CXCR4 inhibitor had clinical diagnoses identical to those in the present study, for example, ovarian, lung, or pancreatic cancer (all demonstrating $SUV_{max} > 6$). As such, a baseline ^{68}Ga-Pentixafor PET/CT revealing increased CXCR4 expression at disease sites may allow identification of patients who would most likely be suitable for nonradiolabeled CXCR4-directed drugs, including LY2510924 (*36*). This would then further expand the theranostic concept beyond identifying patients for treatment with β-emitters, but also to selecting individuals for nonradiolabeled CXCR4-targeted therapeutic options.

Our study has several limitations. We included both CT- and MR-based hybrid imaging, which may provide an additional variable that could be controlled better in future studies. Despite investigating the largest cohort to date, prospective trials should also be undertaken. In addition, the numbers of investigated patients per tumor entity substantially varied. Thus, resulting low numbers of cases and inter- and intrapatient heterogeneity of in vivo CXCR4 expression may have biased the results presented herein. Future studies should therefore consider more balanced subgroups enrolling comparable numbers of patients diagnosed with the identical tumor entity.

CONCLUSION

We found high uptake and image contrast for a variety of neoplasms imaged with ^{68}Ga-Pentixafor PET, such as MM and MCL, but also for adrenal neoplasms and SCLC. These results suggest clinical scenarios in which ^{68}Ga-Pentixafor PET may prove beneficial for directing CXCR4-targeted therapies.

DISCLOSURE

Hans-Jürgen Wester is founder and shareholder of Scintomics. Anja Zehndner is an employee of Pentixapharm, Würzburg. No potential conflict of interest relevant to this article was reported.

KEY POINTS

QUESTION: What is the tracer avidity of malignant lesions, and what are the most avid tumors for CXCR4-targeted ^{68}Ga-Pentixafor PET?

PERTINENT FINDINGS: We observed high uptake and image contrast of the radiopharmaceutical, in particular for hematologic malignancies as well as adrenal neoplasms and small cell lung cancer. Specific activity had no effect on ^{68}Ga-Pentixafor uptake.

IMPLICATIONS FOR PATIENT CARE: Among a broad spectrum of neoplasms, the present bicentric study suggests entities eligible for CXCR4-directed molecular imaging and therapy.

REFERENCES

1. Zlotnik A, Burkhardt AM, Homey B. Homeostatic chemokine receptors and organ-specific metastasis. *Nat Rev Immunol.* 2011;11:597–606.
2. Azad BB, Chatterjee S, Lesniak WG, et al. A fully human CXCR4 antibody demonstrates diagnostic utility and therapeutic efficacy in solid tumor xenografts. *Oncotarget.* 2016;7:12344–12358.
3. Nimmagadda S, Pullambhatla M, Stone K, Green G, Bhujwalla ZM, Pomper MG. Molecular imaging of CXCR4 receptor expression in human cancer xenografts with [^{64}Cu]AMD3100 positron emission tomography. *Cancer Res.* 2010;70:3935–3944.
4. De Silva RA, Peyre K, Pullambhatla M, Fox JJ, Pomper MG, Nimmagadda S. Imaging CXCR4 expression in human cancer xenografts: evaluation of monocyclam ^{64}Cu-AMD3465. *J Nucl Med.* 2011;52:986–993.
5. Yan X, Niu G, Wang Z, et al. Al[^{18}F]NOTA-T140 peptide for noninvasive visualization of CXCR4 expression. *Mol Imaging Biol.* 2016;18:135–142.
6. Demmer O, Gourni E, Schumacher U, Kessler H, Wester HJ. PET imaging of CXCR4 receptors in cancer by a new optimized ligand. *ChemMedChem.* 2011;6:1789–1791.
7. Herrmann K, Lapa C, Wester HJ, et al. Biodistribution and radiation dosimetry for the chemokine receptor CXCR4-targeting probe ^{68}Ga-pentixafor. *J Nucl Med.* 2015;56:410–416.
8. Lapa C, Schreder M, Schirbel A, et al. [^{68}Ga]Pentixafor-PET/CT for imaging of chemokine receptor CXCR4 expression in multiple myeloma: comparison to [^{18}F]FDG and laboratory values. *Theranostics.* 2017;7:205–212.
9. Lapa C, Luckerath K, Rudelius M, et al. [^{68}Ga]Pentixafor-PET/CT for imaging of chemokine receptor 4 expression in small cell lung cancer–initial experience. *Oncotarget.* 2016;7:9288–9295.
10. Derlin T, Jonigk D, Bauersachs J, Bengel FM. Molecular imaging of chemokine receptor CXCR4 in non-small cell lung cancer using ^{68}Ga-pentixafor PET/CT: comparison with ^{18}F-FDG. *Clin Nucl Med.* 2016;41:e204–e205.
11. Werner RA, Kircher S, Higuchi T, et al. CXCR4-directed imaging in solid tumors. *Front Oncol.* 2019;9:770.
12. Weich A, Werner RA, Buck AK, et al. CXCR4-directed PET/CT in patients with newly diagnosed neuroendocrine carcinomas. *Diagnostics (Basel).* 2021;11:605.

13. Bluemel C, Hahner S, Heinze B, et al. Investigating the chemokine receptor 4 as potential theranostic target in adrenocortical cancer patients. *Clin Nucl Med.* 2017; 42:e29–e34.
14. Zhou X, Dierks A, Kertels O, et al. ^{18}F-FDG, ^{11}C-methionine, and ^{68}Ga-pentixafor PET/CT in patients with smoldering multiple myeloma: imaging pattern and clinical features. *Cancers (Basel).* 2020;12:2333.
15. Pan Q, Cao X, Luo Y, Li J, Feng J, Li F. Chemokine receptor-4 targeted PET/CT with ^{68}Ga-pentixafor in assessment of newly diagnosed multiple myeloma: comparison to ^{18}F-FDG PET/CT. *Eur J Nucl Med Mol Imaging.* 2020;47:537–546.
16. Herrmann K, Schottelius M, Lapa C, et al. First-in-human experience of CXCR4-directed endoradiotherapy with ^{177}Lu- and ^{90}Y-labeled pentixather in advanced-stage multiple myeloma with extensive intra- and extramedullary disease. *J Nucl Med.* 2016;57:248–251.
17. Lapa C, Hanscheid H, Kircher M, et al. Feasibility of CXCR4-directed radioligand therapy in advanced diffuse large b-cell lymphoma. *J Nucl Med.* 2019;60:60–64.
18. Maurer S, Herhaus P, Lippenmeyer R, et al. Side effects of CXC-chemokine receptor 4-directed endoradiotherapy with pentixather before hematopoietic stem cell transplantation. *J Nucl Med.* 2019;60:1399–1405.
19. Keller T, Lopez-Picon FR, Krzyczmonik A, et al. Comparison of high and low molar activity TSPO tracer [^{18}F]F-DPA in a mouse model of Alzheimer's disease. *J Cereb Blood Flow Metab.* 2020;40:1012–1020.
20. Lapa C, Kircher S, Schirbel A, et al. Targeting CXCR4 with [^{68}Ga]Pentixafor: a suitable theranostic approach in pleural mesothelioma? *Oncotarget.* 2017;8:96732–96737.
21. Lewis R, Habringer S, Kircher M, et al. Investigation of spleen CXCR4 expression by [^{68}Ga]Pentixafor PET in a cohort of 145 solid cancer patients. *EJNMMI Res.* 2021;11:77.
22. Kraus S, Dierks A, Rasche L, et al. ^{68}Ga-pentixafor-PET/CT imaging represents a novel approach to detect chemokine receptor CXCR4 expression in myeloproliferative neoplasms. *J Nucl Med.* 2022;63:96–99.
23. Werner RA, Weich A, Higuchi T, et al. Imaging of chemokine receptor 4 expression in neuroendocrine tumors: a triple tracer comparative approach. *Theranostics.* 2017;7:1489–1498.
24. Philipp-Abbrederis K, Herrmann K, Knop S, et al. In vivo molecular imaging of chemokine receptor CXCR4 expression in patients with advanced multiple myeloma. *EMBO Mol Med.* 2015;7:477–487.
25. Habringer S, Lapa C, Herhaus P, et al. Dual targeting of acute leukemia and supporting niche by CXCR4-directed theranostics. *Theranostics.* 2018;8: 369–383.
26. Duell J, Krummenast F, Schirbel A, et al. Improved primary staging of marginal-zone lymphoma by addition of CXCR4-directed PET/CT. *J Nucl Med.* 2021;62: 1415–1421.
27. Lapa C, Herrmann K, Schirbel A, et al. CXCR4-directed endoradiotherapy induces high response rates in extramedullary relapsed multiple myeloma. *Theranostics.* 2017;7:1589–1597.
28. Li X, Heber D, Leike T, et al. [^{68}Ga]Pentixafor-PET/MRI for the detection of chemokine receptor 4 expression in atherosclerotic plaques. *Eur J Nucl Med Mol Imaging.* 2018;45:558–566.
29. Vag T, Gerngross C, Herhaus P, et al. First experience with chemokine receptor CXCR4-targeted PET imaging of patients with solid cancers. *J Nucl Med.* 2016; 57:741–746.
30. Demmer O, Dijkgraaf I, Schumacher U, et al. Design, synthesis, and functionalization of dimeric peptides targeting chemokine receptor CXCR4. *J Med Chem.* 2011; 54:7648–7662.
31. Osl T, Schmidt A, Schwaiger M, Schottelius M, Wester HJ. A new class of PentixaFor- and PentixaTher-based theranostic agents with enhanced CXCR4-targeting efficiency. *Theranostics.* 2020;10:8264–8280.
32. Burger JA, Peled A. CXCR4 antagonists: targeting the microenvironment in leukemia and other cancers. *Leukemia.* 2009;23:43–52.
33. Zhao H, Guo L, Zhao H, Zhao J, Weng H, Zhao B. CXCR4 over-expression and survival in cancer: a system review and meta-analysis. *Oncotarget.* 2015;6:5022–5040.
34. Ghobrial IM, Liu CJ, Zavidij O, et al. Phase I/II trial of the CXCR4 inhibitor plerixafor in combination with bortezomib as a chemosensitization strategy in relapsed/refractory multiple myeloma. *Am J Hematol.* 2019;94:1244–1253.
35. Ludwig H, Weisel K, Petrucci MT, et al. Olaptesed pegol, an anti-CXCL12/SDF-1 Spiegelmer, alone and with bortezomib-dexamethasone in relapsed/refractory multiple myeloma: a phase IIa study. *Leukemia.* 2017;31:997–1000.
36. Galsky MD, Vogelzang NJ, Conkling P, et al. A phase I trial of LY2510924, a CXCR4 peptide antagonist, in patients with advanced cancer. *Clin Cancer Res.* 2014; 20:3581–3588.